Journal of Power Sources 247 (2014) 151–155

Contents lists available at ScienceDirect

Journal of Power Sources

journal homepage: www.elsevier.com/locate/jpowsour

Short communication

Syntheses and electrochemical properties of layered $Li_{0.95}Na_{0.05}Ni_{1/3}Co_{1/3}Mn_{1/3}O_2$ and $LiNi_{1/3}Co_{1/3}Mn_{1/3}O_2$

Chunxia Gong, Weixin Lv, Limin Qu, Oluwatosin Emmanuel Bankole, Guanghua Li, Rui Zhang, Meng Hu, Lixu Lei*

School of Chemistry and Chemical Engineering, Southeast University, Nanjing 211189, China

HIGHLIGHTS

- $Li_{0.95}Na_{0.05}Ni_{1/3}Co_{1/3}Mn_{1/3}O_2$ discharges 250.5 mAh g^{-1} under 27 mA g^{-1}.
- The discharge capacity increased after the cell has been standing still for 3 months.
- It is the first example to substitute partial Li atoms for Na in $LiNi_{1/3}Co_{1/3}Mn_{1/3}O_2$.
- The substitution makes a better material for lithium ion batteries.

ARTICLE INFO

Article history:
Received 25 June 2013
Received in revised form
18 August 2013
Accepted 20 August 2013
Available online 31 August 2013

Keywords:
Li-ion battery
Cathode material
Sodium doped
Ternary material
Self-repairing
Electrochemical properties

ABSTRACT

Phase pure $Li_{0.95}Na_{0.05}Ni_{1/3}Co_{1/3}Mn_{1/3}O_2$ and $LiNi_{1/3}Co_{1/3}Mn_{1/3}O_2$ have been synthesized by calcination of co-precipitated precursors. Scanning electron microscopy shows that the powders are aggregated microplates sized between 100 nm and 300 nm in diameter and 50 nm in thickness. Electrochemical tests show that the $Li_{0.95}Na_{0.05}Ni_{1/3}Co_{1/3}Mn_{1/3}O_2$ discharges initially a much higher capacity under a current density of 27 mA g^{-1} (250.5 mAh g^{-1}) than $LiNi_{1/3}Co_{1/3}Mn_{1/3}O_2$ (155.4 mAh g^{-1}). The discharge capacity at the 70th cycle is 134.8 mAh g^{-1} under a current density of 135 mA g^{-1}, and it increases to 143.1 mAh g^{-1} after the test cell has been standing still for 3 months. The latter cell exhibits better cycle performance with capacity retention of 99.02% after 110 cycles at different current densities, therefore, $Li_{0.95}Na_{0.05}Ni_{1/3}Co_{1/3}Mn_{1/3}O_2$ is capable of self-repairing.

1. Introduction

In recent years, $LiCo_{1/3}Ni_{1/3}Mn_{1/3}O_2$ has been investigated extensively as an alternative to $LiCoO_2$, the currently used cathode material in Li-ion batteries. $LiCo_{1/3}Ni_{1/3}Mn_{1/3}O_2$ is isostructural to $LiCoO_2$, in which cobalt, manganese and nickel are trivalent, tetravalent and divalent cations, respectively [1]; also, it can provide higher energy density and better safety characteristics than $LiCoO_2$ [2,3].

Various synthetic methods have been applied to produce $LiNi_{1/3}Mn_{1/3}Co_{1/3}O_2$, such as supercritical water method [4], template method [5,6], solid-state method [7], modified radiated polymer gel method [8], inverse micro emulsion method [9], hydrothermal method [10,11], modified Pechini method [12], flame spray pyrolysis method [13], sol–gel method [14–17], solvent evaporation method [18,19], co-precipitation method [20–24], and soft chemistry EDTA-based method [25]. Among these methods, co-precipitation and sol–gel methods have been found powerful, economic and facile for large scale production [11,26–27], because the transition-metal ions are precipitated homogeneously and oxidized in the aqueous solution at the molecular level [27].

To improve the performance of $LiNi_{1/3}Mn_{1/3}Co_{1/3}O_2$ for high-power electric devices, surface modification has been attempted. For example, the capacity retention can be increased by coating the material with graphene [9], $[B,Al]_2O_3$ [22], polypyrrole [23], CaF_2 [28], polyamic acid [29], ZnO [30], Cr_2O_3 [31] and LBO glass [32]. The discharging capacity can be raised by coating with Cr_2O_3 [31] and LBO glass [32].

Another method to improve the performance of the materials is doping [33–38]. For example, Cu [14], Zr [24], Mg [25], Y [35], Cr

* Corresponding author. Tel.: +86 25 5209 0620x6421; fax: +86 25 52090618.
E-mail address: lixu.lei@seu.edu.cn (L. Lei).

0378-7753/$ – see front matter © 2013 Elsevier B.V. All rights reserved.
http://dx.doi.org/10.1016/j.jpowsour.2013.08.081

[36], Al [14] [37] and Fe [38] are used to substitute part of Ni, Co or Mn, which can improve the cycle performance of $LiNi_{1/3}Co_{1/3}Mn_{1/3}O_2$. We are especially interested in substitution of Li for Na, because the radius of sodium is bigger than lithium, which may increase the interlayer space and make the intercalation and de-intercalation of lithium faster. To best of our knowledge, there are only two papers on replacing Li with Na. The first was Na-doped $LiFePO_4$/C, which discharges a higher capacity of 155 mAh g^{-1} at 0.2 C and 104 mAh g^{-1} at 10 C than the undoped material (142 mAh g^{-1} at 0.2 C and 57 mAh g^{-1} at 10 C) [39]; the second was $Li_{1.05}Na_{0.05}Ni_{0.2}Co_{0.3}Mn_{0.4}O_2$, which has better capacity retention (92%) than $LiNi_{0.2}Co_{0.3}Mn_{0.4}O_2$ (80%) after 50 cycles at 0.25 C rate [40]. Here we report what we have found on the sodium doped $LiCo_{1/3}Ni_{1/3}Mn_{1/3}O_2$. To make a good comparison, we also synthesize and characterize $LiCo_{1/3}Ni_{1/3}Mn_{1/3}O_2$ by the same method.

2. Experimental

2.1. Preparation of the samples

The precursor was prepared as follows: 10 mmol each of $Ni(NO_3)_2{\cdot}6H_2O$, $Mn(NO_3)_2{\cdot}6H_2O$ and $Co(NO_3)_2{\cdot}6H_2O$ were dissolved in 50 mL of deionized water, then an aqueous solution of 60 mmol of NaOH was added to the solution under vigorous stirring. After having been stirred for 12 h at 50 °C in nitrogen atmosphere, the slurry was filtered, washed for three times, and then dried at room temperature in vacuum.

$LiCo_{1/3}Ni_{1/3}Mn_{1/3}O_2$ (denoted as sample Li hereafter) was prepared by mixing LiOH and the precursor in a molar ratio of 1:1 under grinding in an agate mortar for 20 min at room temperature. The obtained mixture was put into a muffle furnace, and the temperature was raised to 450 °C at a rate of 2 °C min^{-1}. After the temperature was maintained for 5 h, the temperature was raised again to 850 °C and kept for 15 h. The final product was collected after the furnace had been cooled naturally to room temperature.

Sodium doped $LiCo_{1/3}Ni_{1/3}Mn_{1/3}O_2$ (denoted as sample LiNa hereafter) was prepared in the same way as above, but a mixture of LiOH and NaOH in a molar ratio of 95:5 was used instead of sole LiOH.

2.2. Experimental techniques

X-ray diffraction (XRD) was measured on an SHIMADZU XD-3A using Cu Ka radiation, λ = 1.54178 Å and a scanning rate of 10° min^{-1}. The morphologies and microstructures of the products were characterized by a scanning electron microscope (SEM, FESEM Hitachi S-4800 II). Chemical compositions of the samples were determined using an inductively coupled plasma/atomic emission spectrometer (ICP-MS, PE ELAN-9000).

The electrochemical performance of each sample was evaluated with a standard CR2032 coin cell with a lithium disc as the negative electrode, a polypropylene membrane (Celgard 2300) as the separator and 1 M $LiPF_6$ in ethylene carbonate (EC) − dimethyl carbonate (DMC) as the electrolyte. The cathode was prepared by coating a slurry consisting of a sample (80 wt.%), acetylene black (10 wt.%), and poly(vinylidene fluoride) (PVDF) (10 wt.%) dispersed in 1-methyl-2-pyrrolidinone (NMP) onto an aluminum foil with an agate pestle. The cathode was then dried at 100 °C for 24 h in a vacuum drying oven. The mass of the active material in each disc was about 1.5–2.5 mg. All batteries were assembled in an argon-filled glove box.

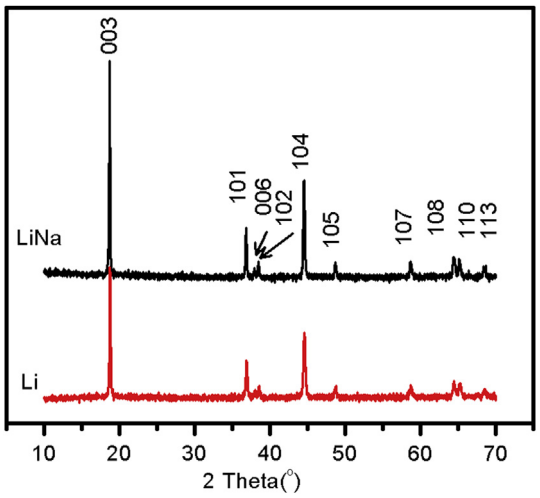

Fig. 1. XRD patterns of the samples.

The charge and discharge tests were performed in the potential range of 2.0–4.5 V at room temperature on a multichannel battery cycling unit (LAND 5.7). Cyclic voltammetry (CV) was determined by an electrochemical workstation (Corrtest CS350) at a sweep rate of 0.5 mV s^{-1}, the reference and auxiliary electrodes were a lithium disc. The electrochemical impedance spectroscopy (EIS) was also done with the coin cell on the electrochemical workstation and a frequency response analyzer controlled by Z-plot. The measurements were performed in the frequency range 100 kHz to 0.001 Hz with AC signal amplitude of 10 mV. Data analysis was done using the software Z view 2.

3. Results and discussion

3.1. Structure and morphology

The elemental analyses of the samples were performed using ICP technique. As indicated in Table 1, the deduced formulas for both samples were $LiNi_{1/3}Co_{1/3}Mn_{1/3}O_2$ and $Li_{0.95}Na_{0.05}Ni_{1/3}Co_{1/3}Mn_{1/3}O_2$ respectively.

Fig. 1 shows the XRD patterns of the samples. For each sample, all the diffraction peaks can be indexed on a hexagonal cell with the space group of *R-3m* as reported [4]. The calculated lattice parameters (*a* and *c*) and standard values of deviation, the *c*/*a* values, and the $I_{(003)}/I_{(104)}$ values are listed in Table 2. It can be seen that the parameters *a* and *c* for sample Li ($LiCo_{1/3}Ni_{1/3}Mn_{1/3}O_2$) are 2.8738 Å and 14.2876 Å; those for sample LiNa ($Li_{0.95}Na_{0.05}Ni_{1/3}Co_{1/3}Mn_{1/3}O_2$) are 2.8748 Å and 14.3009 Å, respectively. Standard values of deviation for *a* and *c* are all smaller than the expanding values (0.0010 Å and 0.0133 Å) by sodium doping, therefore, the lattice expands upon sodium doping. It is known that cation mixing occurs easily in $LiCo_{1/3}Ni_{1/3}Mn_{1/3}O_2$ because the radius of Li^+ (0.076 nm) is

Table 1
The measured elemental contents of the samples with calculated values in brackets.

Sample	Li	Na	Ni	Co	Mn
$LiNi_{1/3}Co_{1/3}Mn_{1/3}O_2$ (Li)	7.19 (7.20)	–	20.61 (20.28)	20.51 (20.36)	18.52 (18.98)
$Li_{0.95}Na_{0.05}Ni_{1/3}Co_{1/3}Mn_{1/3}O_2$ (LiNa)	6.77 (6.78)	1.18 (1.18)	20.74 (20.11)	20.05 (20.20)	18.37 (18.83)

Table 2
Key structural features of the samples with standard values of deviation in brackets.

Synthesized material	Particle size, nm (SEM)	a(Å)	c (Å)	Cell volume (Å)^3	c/a	I_{003}/I_{104}	Tap density (g cm^{-3})
Sample Li	100–300	2.8738 (6)	14.2876 (36)	102.19	4.9717	1.2043	0.8724
Sample LiNa	100–300	2.8748 (3)	14.3009 (14)	102.36	4.9746	1.4499	1.4740

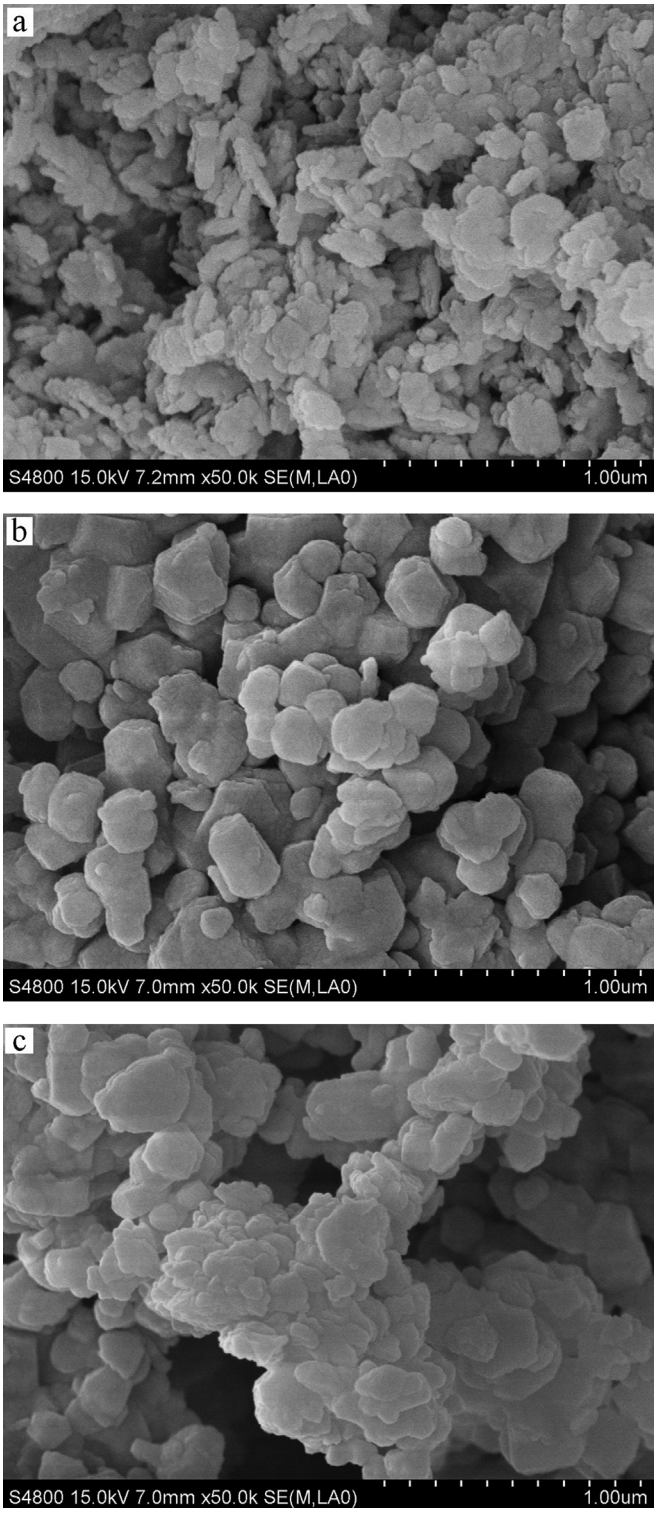

Fig. 2. SEM images of the (a) precursor and (b) sample Li and (c) sample LiNa.

similar to that of Ni^{2+} (0.069 nm); and the greater the values of $I_{(003)}/I_{(104)}$ and c/a, the better the layered structure develops and the less cation mixing occurs [41]. Here, the values of c/a (4.9746) and $I_{(003)}/I_{(104)}$ (1.4499) are a bit higher than those of sample Li (4.9717 and 1.2043), indicating substitution of Na for Li in $LiCo_{1/3}Ni_{1/3}Mn_{1/3}O_2$ can reduce the degree of cation mixing. As it has been known, both Na and Li should occupy 3a site in the samples [42,43].

Fig. 2 shows the SEM images of the precursor and the two samples, and all those are microplates. For the precursor, the average diameter is 200 nm and the thickness is 50 nm. The both samples are more regular than the precursor. The sodium doped sample, LiNa shows smaller average size but severer aggregation. Table 2 also lists the tap densities of the samples, that of sample LiNa is higher than that of sample Li, which may come from the severer aggregation as shown in the SEM image.

3.2. Electrochemical performance

CV was carried out to monitor the electrochemical reactions during charge–discharge process in the voltage range of 2.0–4.5 V at a scan rate of 0.5 mV s^{-1}. As shown in Fig. 3, sample LiNa displays the sharper redox peak and smaller peak potential differences (ΔE) than sample Li. This suggests that faster and better reversibility of the Li intercalation and de-intercalation processes occur on the former electrode [44]. The CV curves of the two samples are similar to that of $LiMn_{1/3}Co_{1/3}Ni_{1/3}O_2$ in a report [45].

Fig. 4 shows the charge–discharge curves of samples Li and LiNa at current densities of 27 mA g^{-1} (0.1 C) and 135 mA g^{-1} (0.5 C). The initial discharge capacities of these two samples are 155.4 and 250.5 mAh g^{-1} at the current density of 27 mA g^{-1}, 86.2 and 153.2 mAh g^{-1} at the current density of 135 mA g^{-1}, respectively. The discharge capacity of sample LiNa is much higher than that of sample Li. This agrees with the CV curves. In a report, the discharge capacity of $Li_{1.1}Ni_{0.2}Co_{0.3}Mn_{0.4}O_2$ also has been improved by doping with Na [40]. Fig. 5 shows the curve of discharged capacities at different rates along with cycle number. It can be seen that sample Li discharges almost nothing at 5 C, but sample LiNa still discharges 37 mAh g^{-1}; therefore sodium doping brings out better high rate performance.

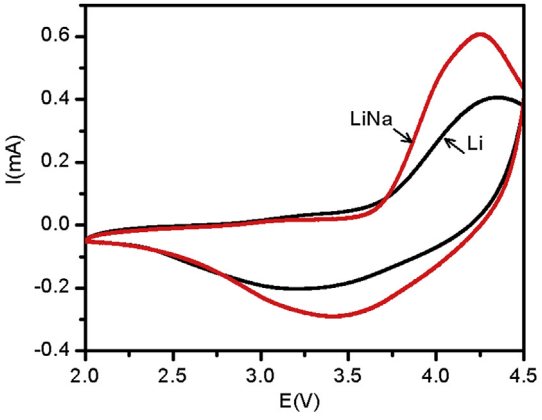

Fig. 3. Cyclic voltammetry of sample Li and sample LiNa.

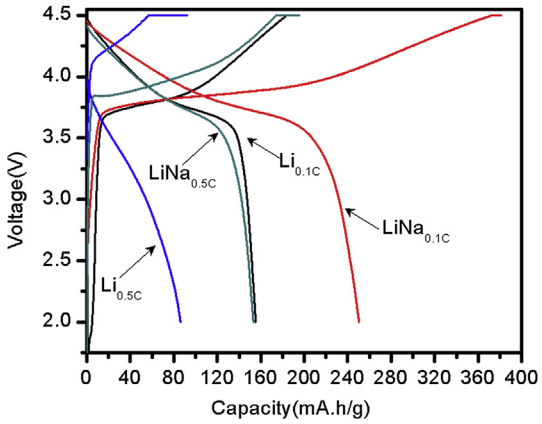

Fig. 4. The charge–discharge curves of the samples.

As we have pointed out in the Section 3.1, sodium doping makes the lattice expand a little, especially the parameter *c*, because the radius of sodium (0.102 nm) is bigger than lithium (0.076 nm). Therefore, sodium doping of the sample LiNa increases the interlayer space and make the intercalation and de-intercalation of lithium easier. As a consequence, the electrochemical performance of the sample LiNa is better than the sample Li, especially at high rate discharging processes. Similar effect has been found in zinc doping of $LiFePO_4$, which enlarges the lattice volume and protects the crystal from shrinking during de-intercalation and intercalation process of lithium ions, because it provides larger space for the movement of lithium ions and improves the electrochemistry performance of $LiFePO_4$ [34].

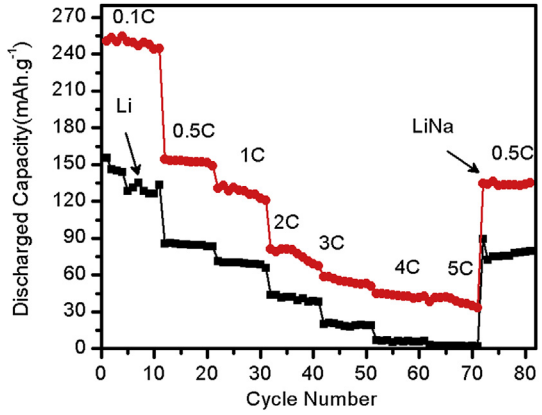

Fig. 5. The cycling behavior of the samples.

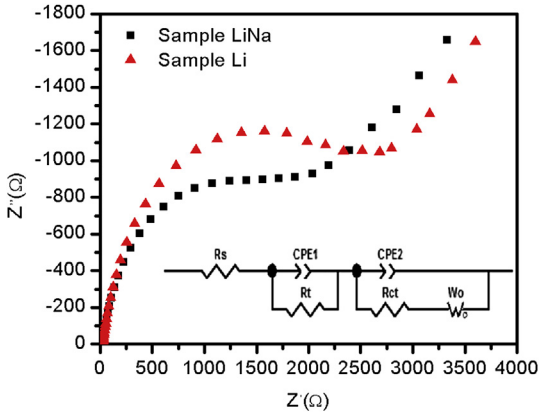

Fig. 6. AC impedance spectra of sample Li and sample LiNa in the frequency range from 100 kHz to 0.01 Hz after 2 V discharged.

Table 3
Impedance analysis of sample Li and sample LiNa.

Samples	Rs	Rt	CPE1	Rct	CPE2	Wo
LiNa	6.734	14.280	2.354e-5	1630	5.005e-3	1285
Li	13.100	8.901	1.193e-5	2377	3.380e-3	1134

The charged capacity of sample LiNa is 381.5 mAh g^{-1} in the first cycle, but the discharged capacity is only 250.5 mAh g^{-1}, therefore, there is the first irreversible capacity (131.0 mAh g^{-1}). The charged capacity is much bigger than the theoretical capacity (270 mAh g^{-1}), we believe that part of the charged capacity comes from the oxidation of the impurities in the test cell [21,46]. Also, it is possible that some of the active materials cannot be reduced during discharge due to poorer electric contact [47,48].

Fig. 6 shows the Nyquist plots of the samples after 80 charge–discharge cycles between 2 V and 4.5 V at the current density of 27 mA g^{-1}, and Table 3 lists the parameters for the simulated circuit. It is clear that the charge-transfer resistance of sample LiNa is smaller than that of sample Li, which again shows that sodium doping improves the kinetic behavior of intercalation and de-intercalation of Li^+.

3.3. Self-repairing capability of the battery

We have tested again a cell (which will be called as 3-month cell hereafter) that had been standing for 3 months after 70 charge–discharge cycles. Fig. 7 shows the cycling behavior at various rates of discharge between 2.0 V and 4.5 V. The initial discharge capacity of the 3-month cell (143.1 mAh g^{-1}) is higher than that of the 70th cycle discharge capacity of the newly made cell (134.8 mAh g^{-1}) at the current density of 135 mA g^{-1}. The newly made cell faded quickly with about 2.51% in the first ten runs. The cycling performance of the 3-month cell was much better; the total capacity retention is 99% in another 110 cycles. Therefore, the cell which uses sample LiNa as cathode material has self-repairing capability, which means aging is good for the material.

The CV curves of the newly made cell and 3-month cell which used sample LiNa as the cathode material are shown in Fig. 8. It can be seen that the CV curves of the 3-month cell shows better symmetry and stronger redox peaks, which means that its cycling performance is improved.

Fig. 9 shows the Nyquist plots of the 3-month cell and the newly made cell after 80 charge–discharge cycles at the current density of 135 mA g^{-1}. The inset shows the enlarged curve for Z′ from 5 Ω to

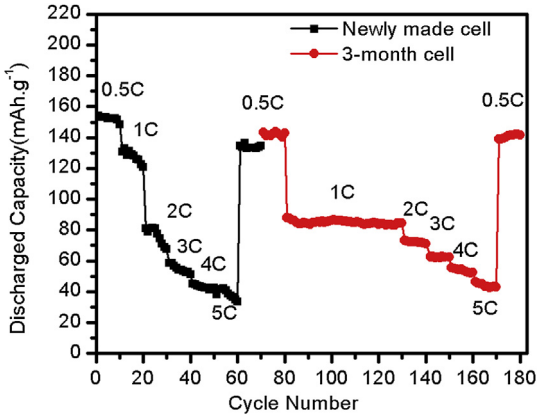

Fig. 7. Cycling behavior at various discharge rates of both the newly made cell and the 3-month cell.

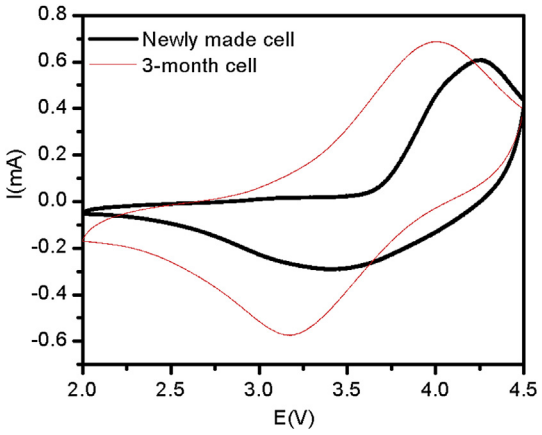

Fig. 8. Cyclic voltammetry of newly made cell and 3-month cell.

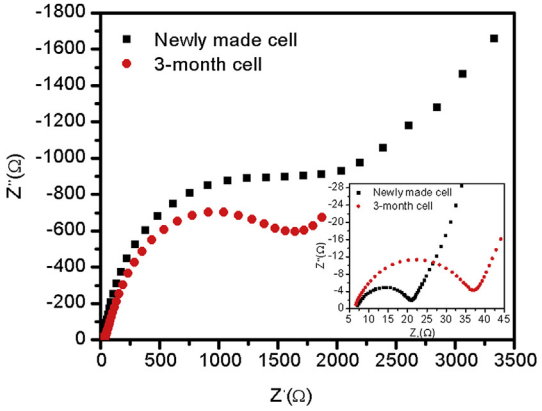

Fig. 9. Nyquist plots of newly made cell and 3-month cell after 2 V discharged.

Table 4
Impedance analysis of newly made cell and 3-month cell.

Cells	Rs	Rt	CPE1	Rct	CPE2	Wo
Fresh made cell	6.734	14.28	2.354e-5	1630	5.005e-3	1285
3-month cell	6.417	29.42	1.606e-5	1366	5.058e-3	271.3

45 Ω. Table 4 lists the parameters for the simulated circuit. It is clear that the charge-transfer resistance of the 3-month cell is smaller than that of the newly made one. The 3-month cell shows faster Li^+ kinetic behavior and better charge–discharge performance.

4. Conclusions

Samples of a ternary Li-ion battery cathode material, $LiNi_{1/3}Co_{1/3}Mn_{1/3}O_2$ (the sample Li) and its sodium doped material $Li_{0.95}Na_{0.05}Ni_{1/3}Co_{1/3}Mn_{1/3}O_2$ (the sample LiNa) have been successfully synthesized by baking a co-precipitated precursor, $NiCoMn(OH)_6$ with LiOH or a mixture of LiOH and NaOH. Both samples are aggregated microplates, but sodium doped one is severer aggregated.

Sodium doping makes the structure more regular and the cation mixing of Li^+ and Ni^{2+} lighter. Also, the separation of MO_2 layer becomes bigger, which makes Li^+ easier to migrate in between the layer and out of the layer. That is the reason why the sodium doped sample discharges much greater capacity at various rates, especially at the high rates. Interestingly, if the sample in the test cell has been aged for 3 months, it shows better cycling performance.

Acknowledgments

We would like to thank The Office of Personnel, Jiangsu Province and The Southeast University for financial supports.

References

[1] T. Ohzuku, Y. Makimura, Chem. Lett. (2001) 642–643.
[2] K.M. Shaju, G.V.S. Rao, B.V.R. Chowdari, Electrochim. Acta 48 (2002) 145–151.
[3] Y. Koyama, I. Tanaka, H. Adachi, Y. Makimura, T. Ohzuku, J. Power Sources 119 (2003) 644–648.
[4] J.W. Lee, J.H. Lee, T.T. Viet, J.Y. Lee, J.S. Kim, C.H. Lee, Electrochim. Acta 55 (2010) 3015–3021.
[5] N.N. Sinha, N. Munichandraiah, J. Electrochem Soc. 157 (2010) A647–A653.
[6] Y.P. Wu, F. Wang, S. Xiao, Z. Chang, Y. Yang, Chem. Commun. (2013), http://dx.doi.org/10.1039/C3CC44360D.
[7] L. Tan, H.W. Liu, Solid State Ionics 181 (2010) 1530–1533.
[8] J.W. Wen, D.W. Zhang, Y.C. Teng, C.H. Chen, Y. Xiong, Electrochim. Acta 55 (2010) 2306–2310.
[9] C.V. Rao, A.L.M. Reddy, Y. Ishikawa, P.M. Ajayan, Acs Appl. Mat Interfaces 3 (2011) 2966–2972.
[10] J.L. Xie, X.A. Huang, Z.B. Zhu, J.H. Dai, Ceramics Int. 36 (2010) 2485–2487.
[11] Y.F. Su, F. Wu, M. Wang, L.Y. Bao, S. Chen, J. Power Sources 195 (2010) 2362–2367.
[12] X.M. Liu, W.L. Gao, B.M. Ji, J. Sol-Gel Sci. Technol. 61 (2012) 56–61.
[13] J.H. Kim, J.H. Yi, Y.N. Ko, Y.C. Kang, Mater. Chem. Phys. 134 (2012) 254–259.
[14] J. Molenda, A. Milewska, M. Molenda, Solid State Ionics 192 (2011) 313–320.
[15] Y.K. Zhou, Y.Y. Hu, J. Wang, Z.P. Shao, Mater. Chem. Phys. 129 (2011) 296–300.
[16] Z.D. Huang, X.M. Liu, B.A. Zhang, S.W. Oh, P.C. Ma, J.K. Kim, Scr. Mater. 64 (2011) 122–125.
[17] Z.D. Huang, X.M. Liu, S.W. Oh, B.A. Zhang, P.C. Ma, J.K. Kim, J. Mater. Chem. 21 (2011) 10777–10784.
[18] H.B. Ren, X.Y. Liu, H.P. Zhao, Z.H. Peng, Y.H. Zhou, Int. J. Electrochem. Sci. 6 (2011) 727–738.
[19] H.B. Ren, X. Lie, Z.H. Peng, Electrochim. Acta 56 (2011) 7088–7091.
[20] H.W. Liu, L. Tan, Mater. Chem. Phys. 129 (2011) 729–732.
[21] Y.S. Lee, K.S. Lee, Y.K. Sun, Y.M. Lee, D.W. Kim, J. Power Sources 196 (2011) 6997–7001.
[22] T.E. Hong, E.D. Jeong, S.R. Baek, M.R. Byeon, Y.S. Lee, F.N. Khan, H.S. Yang, J. Appl. Electrochem. 42 (2012) 41–46.
[23] P.X. Zhang, L. Zhang, X.Z. Ren, Q.H. Yuan, J.H. Liu, Q.L. Zhang, Synth. Met. 161 (2011) 1092–1097.
[24] C.X. Ding, Y.C. Bai, X.Y. Feng, C.H. Chen, Solid State Ionics 189 (2011) 69–73.
[25] J.B. Li, Y.L. Xu, L.L. Xiong, J.P. Wang, Acta Phys. Chim. Sin. 27 (2011) 2593–2599.
[26] R. Santhanam, B. Rambabu, J. Power Sources 195 (2010) 4313–4317.
[27] A.M.A. Hashem, A.E. Abdel-Ghany, A.E. Eid, J. Trottier, K. Zaghib, A. Mauger, C.M. Julien, J. Power Sources 196 (2011) 8632–8637.
[28] K. Xu, Z. Jie, R. Li, Z. Chen, S. Wu, J. Gu, J. Chen, Electrochim. Acta 60 (2012) 130–133.
[29] J.H. Park, J.H. Cho, S.B. Kim, W.S. Kim, S.Y. Lee, J. Mater. Chem. 22 (2012) 12574–12581.
[30] L. Tan, H.W. Liu, Russ. J. Electrochem. 47 (2011) 156–160.
[31] X.W. Li, Y.B. Lin, Y. Lin, H. Lai, Z.G. Huang, Rare Met. 31 (2012) 140–144.
[32] J.Q. Dou, X.Y. Kang, T. Wumaier, H.W. Yu, N. Hua, Y. Han, G.Q. Xu, J. Solid State Electrochem. 16 (2012) 1481–1486.
[33] Y.P. Wu, E. Rahm, R. Holze, Electrochim. Acta 47 (2002) 3491–3507.
[34] H. Liu, Q. Cao, L.J. Fu, C. Li, Y.P. Wu, H.Q. Wu, Electrochem. Commun. 8 (2006) 1553–1557.
[35] Y.W. Li, Y.X. Li, S.K. Zhong, F.P. Li, J.W. Yang, Integr. Ferroelectr. 127 (2011) 150–156.
[36] M.H. Jaafar, N.S. Mohamed, R. Yahya, N. Kamarulzaman, Int. Congress Adv. Appl. Phys. Mater. Sci. 1400 (2011) 280–285.
[37] Y.H. Ding, P. Zhang, Z.L. Long, Y. Jiang, F. Xu, J. Alloys Compd. 487 (2009) 507–510.
[38] H.J. Li, G. Chen, B. Zhang, J. Xu, Solid State Commun. 146 (2008) 115–120.
[39] Z.H. Wang, L.X. Yuan, M. Wu, D. Sun, Y.-H. Huang, Electrochim. Acta 56 (2011) 8477–8483.
[40] S.H. Park, S.S. Shin, Y.K. Sun, Mater. Chem. Phys. 95 (2006) 218–221.
[41] X. Zhang, C. Yu, X. Huang, J. Zheng, X. Guan, D. Luo, L. Li, Electrochim. Acta 81 (2012) 233–238.
[42] H.J. Guo, X.Q. Li, F.Y. He, X.H. Li, Z.X. Wang, W.J. Wang, W.J. Peng, Trans. Nonferrous Met Soc. China 20 (2010) 1043–1048.
[43] S.M. Dou, W.L. Wang, J. Solid State Electrochem. 15 (2011) 399–404.
[44] S.Y. Yang, X.Y. Wang, Q.Q. Chen, X.K. Yang, J.J. Li, Q.L. Wei, J. Solid State Electrochem. 16 (2012) 481–490.
[45] P. Gao, G. Yang, H.D. Liu, L. Wang, H.S. Zhou, Solid State Ionics 207 (2012) 50–56.
[46] J.M. Zheng, D.R. Zhu, Y. Yang, Y.S. Fung, Electrochim. Acta 59 (2012) 14–22.
[47] V.B. Andrew, L.J. Krause, J.R. Dahn, J. Electrochem. Soc. 158 (2011) A731–A735.
[48] Y.Q. Chang, H. Li, L. Wu, T.H. Lu, J. Power Sources 68 (1997) 187–190.